# Effective Diffusivity in Baroclinic Flow

ERIC M. LEIBENSPERGER* AND R. ALAN PLUMB

*Program in Atmospheres, Oceans, and Climate, Department of Earth, Atmospheric and Planetary Sciences, Massachusetts Institute of Technology, Cambridge, Massachusetts*

(Manuscript received 15 July 2013, in final form 12 November 2013)

ABSTRACT

Large-scale chaotic stirring stretches tracer contours into filaments containing fine spatial scales until small-scale diffusive processes dissipate tracer variance. Quantification of tracer transport in such circumstances is possible through the use of Nakamura's ''effective diffusivity'' diagnostics, which make clear the controlling role of stirring, rather than small-scale dissipation, in large-scale transport. Existing theory of effective diffusivity is based on a layerwise approach, in which tracer variance is presumed to cascade via horizontal (or isentropic) stirring to small-scale horizontal (or isentropic) diffusion. In most geophysical flows of interest, however, baroclinic shear will tilt stirred filamentary structures into almost-horizontal sheets, in which case the thinnest dimension is vertical; accordingly, it will be vertical (or diabatic) diffusion that provides the ultimate dissipation of variance. Here new theoretical developments define effective diffusivity in such flows. In the frequently relevant case of isentropic stirring, it is shown that the theory is, in most respects, unchanged from the case of isentropic diffusion: effective isentropic diffusivity is controlled by the isentropic stirring and, it is argued, largely independent of the nature of the ultimate dissipation. Diabatic diffusion is not amplified by the stirring, although it can be modestly enhanced through eddy modulation of static stability. These characteristics are illustrated in numerical simulations of a stratospheric flow; in regions of strong stirring, the theoretical predictions are well supported, but agreement is less good where stirring is weaker.

## 1. Introduction

Transport of tracers in large-scale atmospheric and oceanic flows is often described as a two-dimensional process, in which, through chaotic stirring, tracer variance cascades down to small scales at which diffusion—whether via molecular or small-scale turbulent processes—takes effect. A particularly clear and useful quantitative description of transport in a given two-dimensional flow was given by Nakamura (1996, hereafter N96, 1998, hereafter N98) [and also by Winters and D'Asaro (1996)], who showed that, in a two-dimensional cascade to ultimate two-dimensional diffusivity $\kappa$, net transport is diffusive with an ''effective diffusivity'' $K_{\text{eff}} = \alpha\kappa$, where $\alpha$ is proportional to the square of the ratio of the ''equivalent length'' of tracer contours to their reference (unstretched) length. Under chaotic advection, tracer contours are stretched by the strain in the flow and $\alpha$ becomes large. The arrest of the variance cascade occurs at the ''Batchelor scale'' $b \sim \sqrt{\kappa/\Lambda}$, when thinning of tracer filaments by the large-scale strain $\Lambda$ is balanced by small-scale diffusion. For sufficiently small $b$, one expects the length of tracer contours to be proportional to $b^{-1}$ (so as to preserve area) and hence the equivalent length to vary as $\kappa^{-1/2}$. Then, $K_{\text{eff}}$ becomes independent of $\kappa$ and transport is controlled by large-scale stirring rather than by small-scale diffusion (Shuckburgh and Haynes 2003; Marshall et al. 2006). Application of this theory to modeled and observed atmospheric flows has been discussed by Nakamura and Ma (1997), Haynes and Shuckburgh (2000a), Haynes and Shuckburgh (2000a,b), Allen and Nakamura (2001), and Kostrykin and Schmitz (2006) and to oceanic flows by Marshall et al. (2006), Cerovecki et al. (2009), and Abernathy et al. (2010).

In almost all circumstances, however, the underlying framework of these calculations is not a realistic representation of the termination of the cascade in large-scale atmospheric and oceanic flows. While such flows are

* Current affiliation: Center for Earth and Environmental Science, State University of New York at Plattsburgh, Plattsburgh, New York.

*Corresponding author address:* Eric M. Leibensperger, 101 Broad Street, Plattsburgh, NY 12901.
E-mail: eric.leibensperger@plattsburgh.edu

DOI: 10.1175/JAS-D-13-0217.1

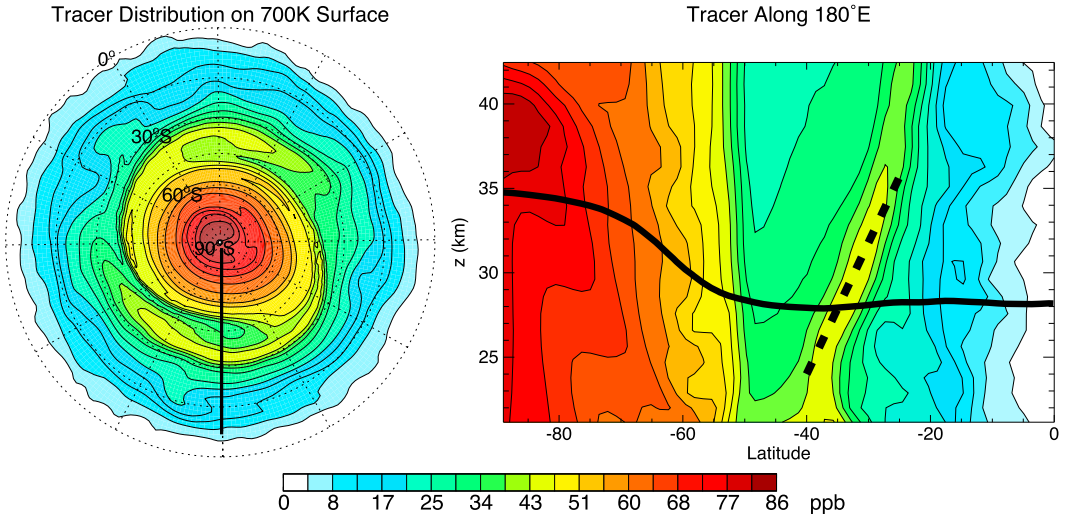


FIG. 1. (left) Tracer distribution on 700-K surface and (right) cross section along 180° from a simulation conducted with T85 horizontal resolution and 100 vertical levels. The dashed line represents the theoretical slope of the tilted filament, the local value of the Prandtl ratio, while the solid line represents the 700-K isentrope. The tracer simulation is discussed in section 3.

indeed almost two-dimensional (in the sense of being quasi horizontal or quasi isentropic) they are usually also baroclinic. As the isentropic strain effects a cascade of tracer variance to small horizontal scales, the vertical shear tilts such features in the tracer field (see Fig. 2) such that the expected ratio of vertical to horizontal scales, in balanced flow, scales as the Prandtl ratio $f/N$, the ratio of the Coriolis parameter to the buoyancy frequency (e.g., Haynes and Anglade 1997). In the atmosphere, and in the upper ocean, $f/N$ is typically of order $10^{-2}$; vertical scales are therefore much smaller than horizontal scales. Thus, what appear to be filaments on an isentropic cross section are more likely to be vertically thin, quasi-horizontal layers. Figure 1 shows an example of such a feature simulated by the atmospheric model described in section 3a. The feature has a much narrower vertical than horizontal extent, displaying a tilt approximately equal to the local value of the Prandtl ratio (dashed line in Fig. 1).

The cascade produced by such large-scale quasi-isentropic stirring is typically arrested by small-scale diffusion that is more isotropic than the large-scale flow. Whenever the ratio of diabatic to isentropic diffusivities is greater than the square of the aspect ratio of filamentary structures [i.e., $(f/N)^2$], vertical (diabatic) diffusion will dominate the dissipation of variance by acting on the small vertical scales (as indicated in Fig. 2). In this paper, we investigate the implications of this fact for our theories of large-scale transport. It is argued that for a given large-scale flow the horizontal (isentropic) effective diffusivity will be independent of whether $\kappa$ acts horizontally or vertically.

A related, and equally important, question is whether the effects of large-scale stirring and tilting enhance transport across, as well as within, isentropic surfaces. Figure 2 might suggest that diabatic transport is enhanced by the generation of small vertical scales. Given the potential importance of even a modest augmentation of the effects of small-scale diabatic transport in stably stratified environments like the stratosphere or the ocean, where diabatic transport is otherwise weak, the question is an important one.

Theoretical developments, including the derivation of an expression for the net isentropic transport (based on the formalism of Nakamura, but with some minor modifications) for the case in which the cascade of tracer variance is arrested by isotropic diffusion, are presented in section 2. The predictions of this theory are illustrated by results from explicit numerical simulations of tracer transport in a modeled stratosphere in section 3. We

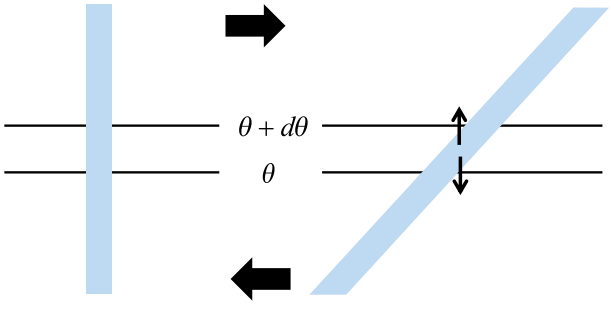


FIG. 2. Illustration of the tilting of narrow filaments to generate small vertical scales. The broad arrows indicate baroclinic shear; the thin arrows depict diabatic tracer diffusion out of the filament.

conclude in section 4 by discussing the general applicability of our results and their implications for the numerical representation of tracer transport.

## 2. Theory

We begin by considering a tracer $q$, governed by the advection–diffusion equation

$$\frac{\partial q}{\partial t} + \mathbf{u}_h \cdot \nabla q + \dot{\theta}\frac{\partial q}{\partial \theta} = \dot{q}, \tag{1}$$

where $\dot{q}$ represents the diffusion that ultimately dissipates tracer variance at small scales. N96 and N98 considered the case where this diffusion occurs isentropically:

$$\dot{q} = \nabla_h(\kappa_i \nabla_h q). \tag{2}$$

Here $\nabla_h$ denotes the components of the gradient operator within the $\theta$ surface and $\kappa_i$ is the isentropic diffusivity. Our focus here is on cases where the ultimate dissipation of variance is dominated by diabatic diffusion, represented by

$$\dot{q} = \frac{1}{\sigma}\frac{\partial}{\partial \theta}\left(\kappa_d \sigma |\nabla\theta|^2 \frac{\partial q}{\partial \theta}\right) = \frac{1}{\sigma}\frac{\partial}{\partial \theta}\left(\kappa_d \sigma \theta_z^2 \frac{\partial q}{\partial \theta}\right), \tag{3}$$

where $\kappa_d$ is the diabatic diffusivity expressed in height coordinates, $\sigma = -g^{-1}\partial p/\partial\theta$ is the $\theta$-coordinate density, and the shallow atmosphere approximation allows $|\nabla\theta|^2 \simeq \theta_z^2$. The term $\sigma$ itself satisfies the continuity equation

$$\frac{\partial \sigma}{\partial t} + \nabla_h \cdot (\sigma \mathbf{u}_h) + \frac{\partial}{\partial \theta}(\sigma\dot{\theta}) = 0. \tag{4}$$

Our analysis mostly follows the modified Lagrangian mean (MLM) approach of N96 and N98, though with some minor notational changes and a somewhat different coordinate system, which makes the form of the MLM tracer budget a little more familiar. The MLM is defined along contours of constant $q = Q$ and on a surface of constant $\theta = \Theta$; N98 then relabels the $Q$ coordinate as an equivalent area coordinate $A_e$ (defined below), expressing the final budget in $(A_e, \Theta)$ coordinates. We make a further trivial step, replacing the area coordinate with a linear variable $Y$, and relabeling the $\Theta$ coordinate with the mean height $Z$ of the $\theta = \Theta$ surface.

Following N98, we consider density-weighted integrals over the area enclosed on a surface of constant $\theta = \Theta$ by a contour $q(x, y, \theta) = Q$. For definiteness, we shall assume that the contour surrounds a maximum of $q$, although the end result is independent of this assumption. Defining the mass integral of any quantity $X$ as

$$\mathcal{M}\{X\} = \iint_{q>Q} \sigma X \, dA, \tag{5}$$

the integrated mass per unit $\Theta$ is

$$M(Q, \Theta, t) = \mathcal{M}\{1\} = \iint_{q>Q} \sigma \, dA. \tag{6}$$

Further, the modified Lagrangian mean—the density-weighted mean around the contour—is defined, following N96 and N98, as

$$\langle X \rangle = \frac{\partial}{\partial Q}(\mathcal{M}\{X\})\left(\frac{\partial M}{\partial Q}\right)^{-1} = \oint \sigma X \frac{dl}{|\nabla_h q|}\left(\oint \sigma \frac{dl}{|\nabla_h q|}\right)^{-1}. \tag{7}$$

Then, again following N98, we apply the operator (5) to (4) to obtain

$$\frac{\partial M}{\partial t} + \frac{\partial}{\partial Q}[\mathcal{M}\{\dot{q}\}] + \frac{\partial}{\partial \Theta}[\mathcal{M}\{\dot{\theta}\}] = 0. \tag{8}$$

Now, we change independent variables from $(Q, \Theta)$ to $(Y, Z)$. Here $Y$ is a latitude-like coordinate, constant along a contour of constant $(Q, \Theta)$, defined as follows. First, we follow N98 in defining an "equivalent area" $A_e$ within a $(Q, \Theta)$ contour such that $M(Q, \Theta) = S(\Theta)A_e$, where $S(\Theta)$ is a representative isentropic density (for our purposes, we define it to be the hemispheric average of $\sigma$ on each $\Theta$ surface). Then, we associate equivalent area with a linear coordinate $Y$ such that $dA_e = L(Y)dY$, where $dY = a d\phi_e$, $\phi_e$ is the "equivalent latitude" (Butchart and Remsberg 1986), the latitude circle containing an area equal to $A_e$,

$$\phi_e = \pm \sin^{-1}\left(1 - \frac{A_e}{2\pi a^2}\right), \tag{9}$$

and

$$L(Y) = \mp 2\pi a \cos\phi_e \tag{10}$$

is the circumference of the latitude circle. The choice of sign depends on the hemisphere of interest. For our purposes, we define area to be that south of the respective $Q$ contour, and so we choose the negative sign in (9) and correspondingly the positive sign in (10). We additionally define the height coordinate $Z(\Theta)$ to be the mean (log pressure) height of the $\theta = \Theta$ surface.

It is a straightforward matter (details are given in appendix B) to show that (8) leads to the following advection–diffusion equation in $(Y, Z)$ coordinates:

$$\frac{\partial Q}{\partial t} + V\frac{\partial Q}{\partial Y} + W\frac{\partial Q}{\partial Z} = \overline{\rho}^{-1}\overline{\nabla}(\overline{\rho}K\overline{\nabla}Q), \tag{11}$$

where $\overline{\nabla} \equiv (\partial/\partial Y, \partial/\partial Z)$, the nondivergent advecting diabatic mean velocity is

$$\mathbf{V} = (V, W) = \frac{1}{\overline{\rho}}\left(-\frac{\partial}{\partial Z}, \frac{\partial}{\partial Y}\right)\mathcal{M}\{\dot{\theta}\} \tag{12}$$

similar to N98, $\overline{\rho}$ is the mass density in $(Y, Z)$ coordinates (defined in appendix A), and the effective diffusivity tensor is

$$\mathbf{K} = \begin{pmatrix} K_{YY} & K_{YZ} \\ K_{ZY} & K_{ZZ} \end{pmatrix}. \tag{13}$$

For the case of ultimate isentropic diffusion [see (2)], $K_{YZ} = K_{ZY} = K_{ZZ} = 0$ and

$$K_{YY} = \langle \kappa_i |\nabla_h q|^2 \rangle \left(\frac{\partial Q}{\partial Y}\right)^{-2} \tag{14}$$

as described by N96 and N98. With diabatic diffusion [see (3)], however, it is shown in appendix B that the effective diffusivity components are[1]

$$\begin{aligned} K_{YY} &= \langle \kappa_d \theta_z^2 q_\theta'^2 \rangle \left(\frac{\partial Q}{\partial Y}\right)^{-2} = \langle \kappa_d q_z'^2 \rangle \left(\frac{\partial Q}{\partial Y}\right)^{-2}, \\ K_{YZ} &= K_{ZY} = \langle \kappa_d \theta_z^2 q_\theta' \rangle \left(\frac{\partial Q}{\partial Y}\frac{d\Theta}{dZ}\right)^{-1}, \\ K_{ZZ} &= \langle \kappa_d \theta_z^2 \rangle \left(\frac{d\Theta}{dZ}\right)^{-2}, \end{aligned} \tag{15}$$

where

$$q_\theta' \equiv \frac{\partial q}{\partial \theta} - \frac{\partial Q}{\partial \Theta} \tag{16}$$

and $q_z' = \theta_z q_\theta'$. Note that $q_\theta'$ is not strictly an eddy term, as there is in general no guarantee that $\langle q_\theta' \rangle = 0$; however, this quantity does in fact vanish if $\sigma$ does not vary on isentropes, as shown in appendix C.

The usefulness and general applicability of expressions like (14) and (15) for diffusivity rely on their independence of the details of each tracer. At first sight, the fact that (14) and $K_{YY}$ and $K_{YZ}$ in (15) involve tracer gradients and the small-scale diffusivities might suggest otherwise. However, note that in each case the diffusivities depend on ratios of the "eddy" tracer gradients to the large-scale isentropic gradients. The former are generated by kinematic folding and tilting of the latter, suggesting that for sufficiently small diffusivity the effective diffusivities are characteristics of the large-scale flow, independent of tracer details. For Nakamura's isentropic diffusivity [see (14)], these issues have been discussed by N96 and, in some detail, by Shuckburgh and Haynes (2003) and Marshall et al. (2006). For sufficiently large Peclet number, $\mathrm{Pe} = \Lambda/(\kappa_i L_0)$, where $\Lambda$ is the rate of stretching by the large-scale flow and $L_0$ a typical length scale of the flow, the cascade of tracer variance is halted at $b \sim \sqrt{\kappa_i/\Lambda} \ll L_0$; in this limit, the effective diffusivity $K_{YY}$ becomes independent of the small-scale diffusivity, and in fact scales as $\Lambda L_0^2$. Marshall et al. (2006) found this limit to be reached when $\mathrm{Pe} \gtrsim 20$.

It is to be anticipated that similar arguments apply to the case with diabatic small-scale diffusion. In fact if we anticipate, following Haynes and Anglade (1997), the vertical and horizontal scales in a mature cascade to be in the Prandtl ratio such that $(q_z')^2 \sim N^2\langle|\nabla_h q'|^2\rangle/f^2$, the isentropic diffusivity becomes

$$K_{YY} \simeq \langle \kappa_d q_z'^2 \rangle \left(\frac{\partial Q}{\partial Y}\right)^{-2} \sim \left\langle \kappa_d \frac{N^2}{f^2} |\nabla_h q|^2 \right\rangle \left(\frac{\partial Q}{\partial Y}\right)^{-2}.$$

Then, the expression for effective isentropic diffusivity $K_{YY}$ in the presence of ultimate vertical diffusion is formally the same as that for ultimate isentropic diffusion with an isentropic diffusivity $\kappa_i = \kappa_d N^2/f^2$. The same arguments about insensitivity of $K_{YY}$ to $\kappa_i$ then apply as in the isentropic case, leading to the expectation that $K_{YY}$ also becomes, in the weak diffusion limit, a measure of large-scale stretching rates. Hence, we might anticipate—and we shall illustrate in model results analyzed in section 3—that $K_{YY}$ becomes largely independent of whether the ultimate dissipation of tracer variance is diabatic or isentropic.

The off-diagonal components of the diffusivity tensor indicate, if nonzero, that the principal axis of effective diffusion does not coincide with the isentropes. One can show that these components are in fact zero if there are no variations of either $\theta_z$ or $\sigma$ within isentropic surfaces: if variations in $\theta_z$ along a tracer contour can be neglected, then $\langle \theta_z^2 q_\theta' \rangle = \langle \theta_z^2 \rangle \langle q_\theta' \rangle$ and, as already noted, $\langle q_\theta' \rangle = 0$ under such circumstances. As will be shown in the next section, while these off-diagonal terms are not zero in our numerical simulations, they are small enough to be of little practical consequence.

[1] The definition of the various components is in fact nonunique: one can manipulate the definitions of the components of $\mathbf{K}$ and of the advecting velocity $\mathbf{V}$ in such a way as to leave the net transport unchanged. (One example of this ambiguity is noted in section 3c.) The definition set that we present here seems to be the simplest and most logical choice.

TABLE 1. Simulations conducted in this study and estimates of vertical and horizontal numerical diffusion. The column labeled "vertical" indicates resolution in model layers and vertical spacing in the stratosphere.

| Resolution | | | |
|---|---|---|---|
| Horizontal | Vertical | $\kappa_h^{\text{num}}$ ($\text{m}^2\,\text{s}^{-1}$) | $\kappa_v^{\text{num}}$ ($\text{m}^2\,\text{s}^{-1}$) |
| T42 (~2.8°) | 80 (1.0 km) | $4.6 \times 10^3$ | 0.8 |
| T63 (~1.9°) | 40 (2.0 km) | $2.4 \times 10^3$ | 1.0 |
| T63 (~1.9°) | 60 (1.5 km) | $2.2 \times 10^3$ | 0.9 |
| T63 (~1.9°) | 80 (1.0 km) | $1.8 \times 10^3$ | 0.8 |
| T63 (~1.9°) | 100 (0.8 km) | $1.4 \times 10^3$ | 0.2 |
| T85 (~1.4°) | 80 (1.0 km) | $1.2 \times 10^3$ | 0.7 |
| T85 (~1.4°) | 100 (0.8 km) | $1.0 \times 10^3$ | 0.2 |

Note that the expression for vertical effective diffusivity $K_{ZZ}$ in (15) is unrelated to the isentropic stirring and baroclinic tilting of tracer contours of the kind illustrated in Fig. 2. Enhancement of diabatic diffusion occurs only through the factor $\langle\theta_z^2\rangle/(d\Theta/dZ)^2$, which is independent of the tracer structures, but rather expresses the impact of modulations of isentropic thickness by the eddies. Unlike the collapse of vertical scales of the tracer variance, there are strong dynamical constraints such as potential vorticity conservation that prevent the sustained collapse of isentropic thickness; nevertheless, the possibility of some enhancement of diabatic mixing in the presence of eddies is indicated by (15) and will be discussed further in what follows.

## 3. Numerical simulation of $K_{YY}$, $K_{YZ}$, and $K_{ZZ}$

### a. Atmospheric model

In this section, we illustrate the theoretical results of section 2 with simulations of atmospheric tracer transport in a simplified general circulation model. Our focus is the stratosphere, building upon prior application of the N98 framework to the middle atmosphere by Haynes and Shuckburgh (2000a), Allen and Nakamura (2001), and Kostrykin and Schmitz (2006). The model is similar to that of Polvani and Kushner (2002), consisting of a dry pseudospectral dynamical core forced by the thermodynamic and momentum parameterizations of Held and Suarez (1994). The model integrates the primitive equations within a hybrid $\sigma$–$p$ vertical coordinate extending from the surface to 0.006 hPa. The hybrid coordinate follows Simmons and Burridge (1981). The $\sigma$ coordinate transitions to the $p$ coordinate between 300 and 100 hPa. Pressure surfaces are distributed such that the number of model layers roughly corresponds to height spacing in the stratosphere. Simulations are conducted at the combinations of horizontal and vertical resolution listed in Table 1. Vertical resolution in the stratosphere varies from 0.8 km (100 levels) to 2.0 km (40 levels). Rayleigh friction is applied below 700 hPa to represent surface drag and above 0.5 hPa to crudely parameterize gravity wave drag within the mesosphere. Temperatures are linearly relaxed to zonal equilibrium profiles; equilibrium temperature profiles used here are similar to those of Held and Suarez (1994) but contain asymmetry about the equator to generate solstice conditions. A polar vortex is formed within the winter hemisphere by imposing a lapse rate in equilibrium temperature $\gamma$ of $4\,\text{K}\,\text{km}^{-1}$ through the polar stratosphere (Polvani and Kushner 2002). A 1000-day spinup is conducted from a static, isothermal initial condition for each resolution.

The model transports tracers horizontally using a semi-Lagrangian advection scheme and vertically with a finite-volume parabolic scheme. Mass conservation is not assured by these schemes, but we enforce it by applying a global "mass fixer." This correction scales the tracer field after each advective time step in order to retain a constant global tracer mass. Test simulations conducted without the mass fixer reveal that its use does not significantly affect our calculation of effective diffusivity. The model's tracer simulation has recently been used to diagnose stratosphere–troposphere exchange (Orbe and Polvani 2012) and the Brewer–Dobson circulation (Gerber 2012).

Two tracers, each containing no source or sink, are simulated in each model integration; small-scale diffusion is applied purely isentropically to one tracer and purely diabatically to the other. Both tracers thus experience the same large-scale stirring but differ in the mechanism dissipating small-scale tracer variance. Additional diffusion arises from the numerical advection routines. We quantify numerical diffusion by calculating the tendency of globally averaged tracer variance (Allen and Nakamura 2001; Abernathy et al. 2010):

$$\frac{1}{2}\frac{\partial\overline{q^2}}{\partial t} = -\kappa_i^{\text{num}}\overline{|\nabla q|^2} - \kappa_v^{\text{num}}\overline{\left(\frac{\partial q}{\partial z}\right)^2}. \qquad (17)$$

Here, the overbar represents the global mass-weighted mean (surface to top of atmosphere). We separately regress the tendency of globally averaged tracer variance against $|\nabla q|^2$ and $(\overline{\partial q}/\partial z)^2$ since horizontal and vertical numerical diffusion cannot be disentangled. As a result, the estimates presented in Table 1 assume that the destruction of tracer variance occurs solely through horizontal or vertical numerical diffusion and are upper limits. Horizontal and vertical numerical diffusion are not strictly independent, but our method is conservative enough to account for any interdependence. As might be expected, the amount of numerical diffusion is greatest for the coarsest simulations and decreases as resolution improves.

An explicit diffusivity of $\kappa_i = 5.0 \times 10^4\,\mathrm{m^2\,s^{-1}}$ is applied to the "isentropic" tracer and $\kappa_d = 1.25\,\mathrm{m^2\,s^{-1}}$ to the "diabatic" tracer. These values are larger than our estimates for numerical diffusion, although only marginally so for the diabatic tracer except in the simulations containing 100 layers. Tracer concentrations are initialized with $q = |\phi|$ (ppb) for $\phi < 0$, where $\phi$ is latitude. Elsewhere, tracer concentrations are initialized with a value of 0.01 ppb. There is no initial vertical structure in the tracer fields. Each tracer simulation is conducted for at least 100 days. The first 30 days of the tracer simulation are discarded to ensure flow diagnostics independent of the initial tracer field (Haynes and Shuckburgh 2000a).

The stratospheric circulation generated in this model, other factors being fixed, depends on the magnitude of planetary-scale topography specified at the surface. For example, wavenumber-2 topography of amplitude 3 km generates large amplitude quasi-stationary Rossby waves sufficient to produce intermittent major warming events of realistic frequency and intensity (Gerber and Polvani 2009). Major warming events, however, are undesirable in our study since such events cause our calculated effective diffusivity to become an average over two stirring regimes: quiescent periods when stirring is mostly confined to the midlatitude surf zone, and warming events during which stirring extends across high latitudes. Accordingly, we choose to focus our calculations on a less disturbed regime by imposing a flat lower boundary in the model. Planetary-scale Rossby waves produced by synoptic wave interactions (Scinocca and Haynes 1998) still appear in the stratosphere but are weak enough that, at least with this model configuration, only weak, minor, warming events are produced. This is not particularly realistic as an analog of the northern winter circulation but is qualitatively similar to the behavior of the southern stratosphere in midwinter. As we shall see, the relatively weak stirring in the middle and upper stratosphere has some consequences for the interpretation of effective diffusivity in the results.

### b. Calculation of effective diffusivity

Effective diffusivity ($K_{YY}$, $K_{YZ}$, $K_{ZZ}$) is calculated using (14) and (15) and daily instantaneous tracer fields. Tracer concentrations are linearly interpolated onto isentropic surfaces extending from 400 to 1500 K with 15-K resolution, defining the $\Theta$ coordinate. The $\Theta$ coordinate is also expressed as the hemispheric-mean log-pressure height $Z$ of each surface. For each isentropic surface, 250 evenly spaced $Q$-contour levels are created between the minimum and maximum tracer concentrations. Each $Q$ contour is mapped onto the horizontal coordinate $Y$ through the contour equivalent area as outlined in section 2. We find that our calculations are not particularly sensitive to the number of tracer contours or isentropic levels used.

The calculation of effective diffusivity is the product of two components: the MLM of the local tracer or $\theta$ gradient, and the inverse square of the large-scale gradient of tracer ($\partial Q/\partial Y$) or potential temperature ($\partial\Theta/\partial Z$). The latter component of the effective diffusivity is a straightforward calculation using finite differences of the mapping of $Q \rightarrow Y$ and $\Theta \rightarrow Z$.

The MLM of a generalized property $\xi$ is calculated as follows. First, a mass-weighted ($\sigma A$, where $A$ is the gridbox area) summation of $\xi$ is conducted within each contour $Q$. A summation of the contour mass is also performed. The MLM is calculated as the ratio of the difference of the weighted summation of $\xi$ across $Q$ contours to the change in mass within the contours. That is, for gridded $\xi$,

$$\langle\xi\rangle(Q,\Theta) = \frac{\sum\limits_{q>Q+\delta Q} \xi(i,j,\Theta)\sigma(i,j,\Theta)A(i,j) - \sum\limits_{q>Q-\delta Q} \xi(i,j,\Theta)\sigma(i,j,\Theta)A(i,j)}{\sum\limits_{q>Q+\delta Q} \sigma(i,j,\Theta)A(i,j) - \sum\limits_{q>Q-\delta Q} \sigma(i,j,\Theta)A(i,j)}, \tag{18}$$

where $i$ and $j$ are the horizontal gridbox indices within the appropriate $Q$ contour. Equation (18) is a discretized version of (7). To apply (18) to (15), the horizontal and vertical gradients of $q$ are calculated for each grid point and daily tracer field. Equation (18) is additionally used to calculate the MLM of the zonal wind.

The key expressions in the first and second of the definitions in (15) for $K_{YY}$ and $K_{YZ}$ can be written, using (16), as

$$\left\langle \left(\frac{\partial\theta}{\partial z}\right)^2 (q'_\theta)^2 \right\rangle (Q,\boldsymbol{\Theta}) = \left\langle \left(\frac{\partial q}{\partial z} - \frac{\partial\theta}{\partial z}\frac{\partial Q}{\partial\Theta}\right)^2 \right\rangle \quad \text{and}$$

$$\left\langle \left(\frac{\partial\theta}{\partial z}\right)^2 q'_\theta \right\rangle (Q,\Theta) = \left\langle \frac{\partial\theta}{\partial z}\left(\frac{\partial q}{\partial z} - \frac{\partial\theta}{\partial z}\frac{\partial Q}{\partial\Theta}\right) \right\rangle,$$

with $z$ denoting the local log-pressure height.

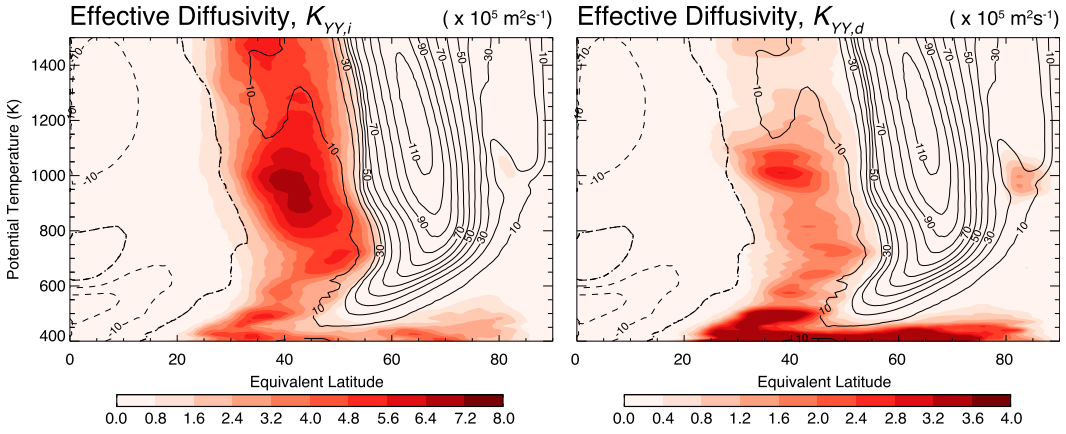


FIG. 3. Effective diffusivity $K_{YY}$ ($\times 10^5$ m$^2$ s$^{-1}$) calculated from a simulation dissipating tracer variance with explicit (left) isentropic ($K_{YY,i}$) or (right) diabatic ($K_{YY,d}$) diffusion. Black contours represent the MLM of the zonal wind (contour interval is 10 m s$^{-1}$; negative values are dashed). Note the difference in color scale between $K_{YY,i}$ and $K_{YY,d}$. The simulation was performed with a horizontal resolution of T85 and 100 vertical levels.

### c. *Numerical modeling results*

The left panel of Fig. 3 shows $K_{YY,i}$, the isentropic diffusivity calculated using (14) and the tracer modeled with isentropic diffusion, along with the MLM of the zonal wind from the simulation with the finest horizontal (T85, ~155 km) and vertical (100 levels, ~0.8 km) spatial resolutions. The distribution of $K_{YY,i}$ is similar to prior estimates for austral winter (Haynes and Shuckburgh 2000a; Allen and Nakamura 2001), but the absolute magnitude is lower in our idealized atmosphere owing to the smaller amount of wave forcing from the imposed flat topography. Small values of $K_{YY,i}$ are found in the tropics and vortex edge, the so-called transport barriers. Tracer contours generally have simpler geometry in these regions with correspondingly small values of effective diffusivity. Values in these regions approach the imposed small-scale diffusivity $\kappa_i$ ($0.5 \times 10^5$ m$^2$ s$^{-1}$). Above the lower stratosphere, the largest values of $K_{YY,i}$ are located equatorward of the polar vortex, where mixing is strong and tracer contours are filamented within the midlatitude surf zone (see Fig. 1). In fact, the largest values of $K_{YY,i}$ are neatly confined between the vortex and the zero zonal wind line. In this region, $K_{YY,i}$ is up to 25 times larger than $\kappa_i$, indicating significant contour stretching and large equivalent lengths. Higher values of $K_{YY,i}$ are evident in a broad latitudinal region of the lower stratosphere where stronger stirring is associated with the upper extensions of synoptic-scale tropospheric eddies.

The right panel of Fig. 3 shows $K_{YY,d}$, the isentropic effective diffusivity calculated using (15), and the tracer with imposed diabatic diffusion. The large-scale structure of $K_{YY,d}$ is similar to that of $K_{YY,i}$; that is, values are largest in the surf zone and lower stratosphere. Within the surf zone, the spatial pattern of $K_{YY,d}$ corresponds well with the features of $K_{YY,i}$, including local maxima at 475 and 800 K, a broad structure between 600 and 1100 K, and a minimum value at 1300 K. Despite the similarities in spatial structure, however, $K_{YY,d}$ and $K_{YY,i}$ differ in magnitude. Figure 4 shows their ratio, $K_{YY,d}/K_{YY,i}$. In line with the theoretical arguments, the ratio is close to unity in the lower stratosphere, below 550 K where stirring is strongest. Elsewhere, $K_{YY,d}$ is generally at least a factor of 2 smaller than $K_{YY,i}$ within the surf zone and much smaller in the transport barriers. This suggests that the conditions in the regions of weaker stirring have not reached those assumed in the theoretical discussion. Sensitivity simulations with differing values of $\kappa_i$ reveal that $K_{YY,i}$ is not entirely independent

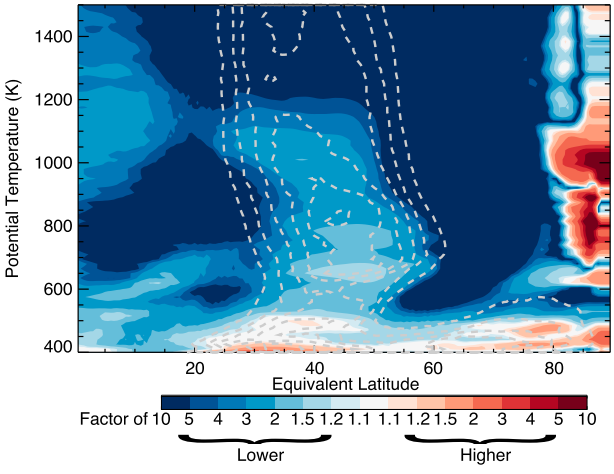


FIG. 4. Ratio of $K_{YY,d}$ to $K_{YY,i}$ from the simulation presented in Fig. 3. Blues (reds) indicate that $K_{YY,d}$ is lower (higher) than $K_{YY,i}$. Dashed lines indicate $K_{YY,i}$ of the control simulation.

of the applied small-scale diffusion, with the largest sensitivity to $\kappa_i$ occurring in the weakly stirred transport barriers and surf zone above 1200 K. This further highlights discrepancies between theory and weakly stirred regions.

In the strongly stirred lower stratosphere, $f/N$ scaling is produced as filamentary structures are rapidly stretched and tilted. It is here that $K_{YY,d}$ is most similar to $K_{YY,i}$. In contrast, the largest discrepancies between $K_{YY,i}$ and $K_{YY,d}$ occur in regions experiencing weakest stirring (i.e., the transport barriers). In these locations $Q$ contours have simple geometry and $|\nabla_h q|^2 \sim (\partial Q/\partial Y)^2$, so that $K_{YY,i} \sim \kappa_i$. However, since there are no finescale filaments to be tilted, the vertical-scale collapse is weak so that $K_{YY,d}$ is much smaller than $K_{YY,i}$. In this situation, diabatic diffusion does not participate in the dissipation of isentropically driven cascade of tracer variance. As a result, weak diabatic diffusion does not have much impact on tracer transport in regions experiencing little wave activity.

Two additional factors complicate the comparison of $K_{YY,i}$ and $K_{YY,d}$: the intermittency of wave activity and the proximity of filaments to the vortex edge. Wave activity is not continuous and thus effective diffusivity is not constant through time. As such, the values presented in Fig. 3 represent average conditions and do not necessarily retain $f/N$ scaling. Also, filaments are commonly formed by stripping tracer away from the polar vortex edge. In this situation, a portion of the length of tracer contours lies along the vortex edge, a location with large horizontal tracer gradients, but not necessarily large vertical gradients. The calculation of effective diffusivity along such a contour is thus partially biased by processes not governed by $f/N$ scaling. These complications are overcome in the lower stratosphere, where the effects of a strong vortex are lacking and wave activity is stronger and much more frequent.

Note the relatively large values of $K_{YY,d}$ within the polar vortex, which are especially evident in the ratio $K_{YY,d}/K_{YY,i}$ shown in Fig. 3. These are indicative not of the stretching–tilting processes of the surf zone, but rather of the impact of small values of $q'_\theta$ in the presence of the small values of $(\partial Q/\partial Y)$ in the calculation of $K_{YY,d}$. Such values are inevitable near the pole where the mean gradient vanishes. As such, these large values of $K_{YY,d}$ exemplify the ambiguities in the representation of $K$ noted earlier. Even in the absence of zonal asymmetries, a vertical diffusive flux

$$\mathbf{F} = -\kappa_z \frac{\partial q}{\partial z}\hat{\mathbf{z}},$$

where $\hat{\mathbf{z}}$ is the upward unit vector, can be written, identically, as the sum of a component along the $q$ contours (which is therefore advective in nature) and a horizontal component

$$\mathbf{F} = \kappa_z \left(\frac{\partial q/\partial z}{\partial q/\partial y}\right)\hat{\mathbf{x}} \times \nabla q - \kappa_z \left(\frac{\partial q/\partial z}{\partial q/\partial y}\right)^2 \frac{\partial q}{\partial y}\hat{\mathbf{y}}, \quad (19)$$

where $\hat{\mathbf{x}}$ and $\hat{\mathbf{y}}$ are, respectively, unit vectors in the $x$ and $y$ directions. Thus, a vertical diffusion can be represented by the sum of an advective flux plus horizontal diffusion. That this is not generally a sensible thing to do is evidenced by the fact that the transfer coefficients in (19) are dependent on the geometry of the tracer isopleths. Provided the isopleth slopes are dictated by the large-scale flow—as they will be in a region of strong stirring—the effective diffusivity is meaningful. This is not the case in the weakly stirred vortex interior, and so the relatively large polar values of $K_{YY,d}$ are misleading. However, given the small absolute values of $K_{YY}$ within the vortex, the point is moot.

Estimates of $K_{YY}$ are sensitive to the resolution of tracer advection: as resolution improves, finer-scale features are resolved and the contour equivalent length increases (Allen and Nakamura 2001). If the discrepancies between $K_{YY,i}$ and $K_{YY,d}$ are due to inadequate resolution of the tracer cascade, one would expect the values to show convergence as resolution is improved. Note that changes in resolution in these calculations apply to the dynamical fields as well as to the tracers; that is, the dynamical simulations change somewhat as resolution is changed (although changes in the flow statistics are modest). Thus, unlike some previous studies, the sensitivity to resolution discussed here is not simply a matter of changing the resolution of tracer transport in a given flow.

The left panels of Fig. 5 show $K_{YY,i}$ at 850 and 450 K for the resolutions listed in Table 1. To ensure meaningful comparisons, $K_{YY,i}$ is averaged over periods (typically 30 days) containing an active surf zone ($K_{YY,i}$ is large). While $K_{YY,i}$ increases with horizontal resolution, it is not as sensitive to improved vertical resolution (dashed lines in Fig. 5). This sensitivity is largest in the surf zone where stirring is modestly vigorous and the representation of filamentary structures benefits from enhanced resolution (Haynes and Shuckburgh 2000a; Allen and Nakamura 2001). The right panels of Fig. 5 show the effect of resolution on the diagnosed value of $K_{YY,d}$. Similar to $K_{YY,i}$, higher resolution increases the estimate of $K_{YY,d}$; not surprisingly, in this case the greater sensitivity is to vertical resolution with a large increase between 60 levels (1.5 km) and 80 levels (1.0 km) at 850 K and between 80 and 100 levels at 450 K, where the length scales are smaller. Agreement between $K_{YY,i}$ and $K_{YY,d}$ improves with increased resolution; at the

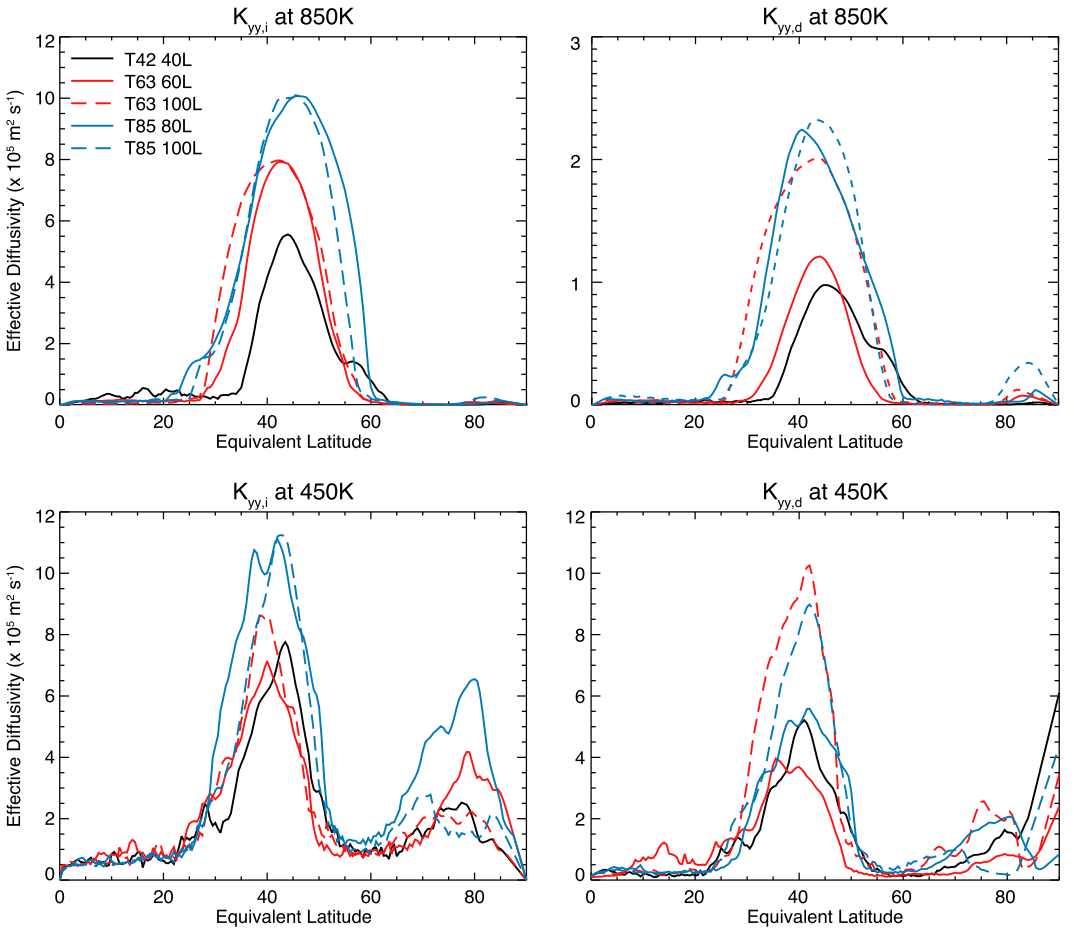


FIG. 5. Effective diffusivity ($\times 10^5\,\mathrm{m^2\,s^{-1}}$) (left) $K_{YY,i}$ and (right) $K_{YY,d}$ on the (top) 850- and (bottom) 450-K isentropic surfaces as calculated from simulations with spatial resolutions: T42, 40 levels (black); T63, 60 levels (red solid); T63, 100 levels (red dashed); T85, 80 levels (blue solid); and T85, 100 levels (blue dashed). Note the difference in scale between $K_{YY,i}$ and $K_{YY,d}$ at 850 K.

highest resolutions used here, agreement is good at 450 K, but at 850 K the discrepancies, though smaller than at lower resolution, remain substantial.

Figure 6 shows $K_{YZ}$ and $K_{ZZ}$ calculated from the same simulation presented in Fig. 3. The left panel of Fig. 6 shows $K_{YZ}$, the off-diagonal component of the effective diffusion tensor in (15). Unlike $K_{YY}$, $K_{YZ}$ has mixed sign throughout the stratosphere. The largest values of up to $80\,\mathrm{m^2\,s^{-1}}$ occur in the lower stratosphere; in the middle and upper stratosphere, typical values are around $10\,\mathrm{m^2\,s^{-1}}$. As mentioned in section 2, theory suggests $K_{YZ}$ to be negligible if variations in $\sigma$ are small within an isentropic surface and, indeed, these values are small. The role of the off-diagonal components is to rotate the principal axes of diffusion through an angle of $K_{YZ}/K_{YY} \sim 10^{-5}$, which corresponds to a slope of the principal diffusion axis relative to isentropes of about 100 m between equator and pole, which can undoubtedly be regarded as negligible (isentropic surfaces themselves slope by factors of 10–100 more than this.)

The right panel of Fig. 6 shows that $K_{ZZ} \approx \kappa_d$ throughout most of the stratosphere, indicating that the enhancement of tracer diffusion due to modulations of isentropic thickness by the eddies is minimal in those places. Within the polar vortex, $K_{ZZ}$ is amplified by a factor of up to 5, but this amplification appears not to be primarily the result of eddy effects. Rather, $K_{ZZ}$ is artificially enhanced as a consequence of using the hemispheric mean height. Isentropic thickness is smaller within the polar vortex than elsewhere, making $\partial\theta/\partial z > \partial\Theta/\partial z$. As a result, $K_{ZZ}$ is amplified there owing to our choice of coordinate system rather than a physical process. Where the eddies are stronger, diabatic diffusivity is not substantially enhanced; thus it appears that the presence of eddies does not significantly enhance diabatic mixing in these simulations.

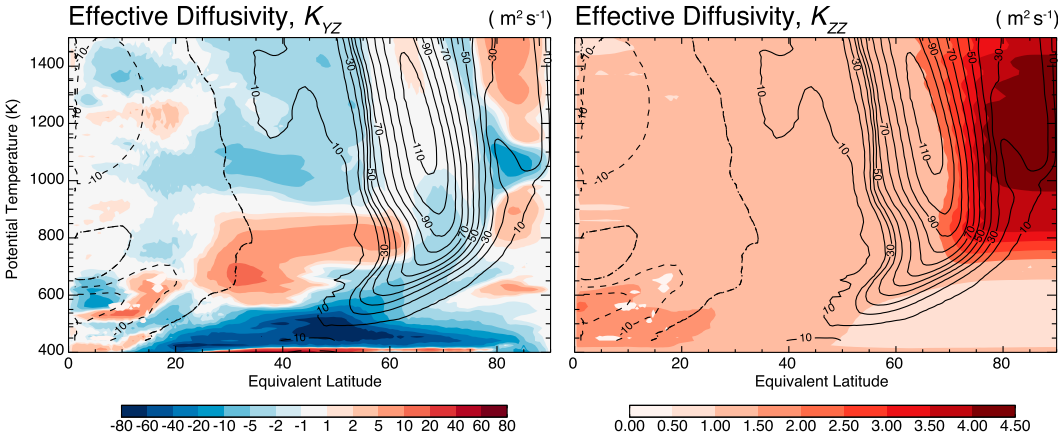


FIG. 6. Effective diffusivity components (left) $K_{YZ}$ ($m^2\,s^{-1}$) and (right) $K_{ZZ}$ ($m^2\,s^{-1}$) calculated from a simulation dissipating tracer variance with explicit diabatic diffusion $\kappa$. Black contours represent the MLM of the zonal wind (contour interval is $10\,m\,s^{-1}$; negative values are dashed). Note the nonlinear color scale of $K_{YZ}$.

The final component of transport is mean advection. The advecting velocity that appears in (11) and in N98 has MLM mass streamfunction

$$\mathcal{M}(Y,Z,t)\{\dot{\theta}\} = \iint \sigma\dot{\theta}\,dA\,, \tag{20}$$

where the integral is over the area poleward of the appropriate equivalent latitude contour (of constant $Q$). This is not the same as the conventional zonal-mean diabatic circulation, which has mass streamfunction also given by (20) but for which the integral is over the area poleward of a circle of constant latitude. The two streamfunctions are compared in Fig. 7. In magnitude and in general shape, the two are similar, although the MLM streamfunction is flatter in the surf zone (with little upwelling or downwelling between 20° and 50° equivalent latitude) and the MLM high-latitude descent closely follows the vortex edge, including the equatorward kink in the edge near 500 K (cf. the MLM wind maximum in Fig. 3).

## 4. Discussion

We have expanded the effective diffusivity diagnostic of N96 and N98 by deriving the equations in the presence of diabatic diffusion. Our derivation produces a solution [see (11)] similar to that of N98, but with the isentropic effective diffusivity (denoted $K_{YY}$) replaced by an effective diffusivity tensor $\mathbf{K}$ that includes not only the isentropic component of effective diffusivity but additionally consists of vertical ($K_{ZZ}$) and off-diagonal components ($K_{YZ}$). Our numerical simulations confirm the theoretical expectation that $K_{YZ}$ is small enough to be negligible, while $K_{ZZ}$ differs little from the imposed diabatic diffusivity $\kappa_d$; thus, diabatic diffusion is not

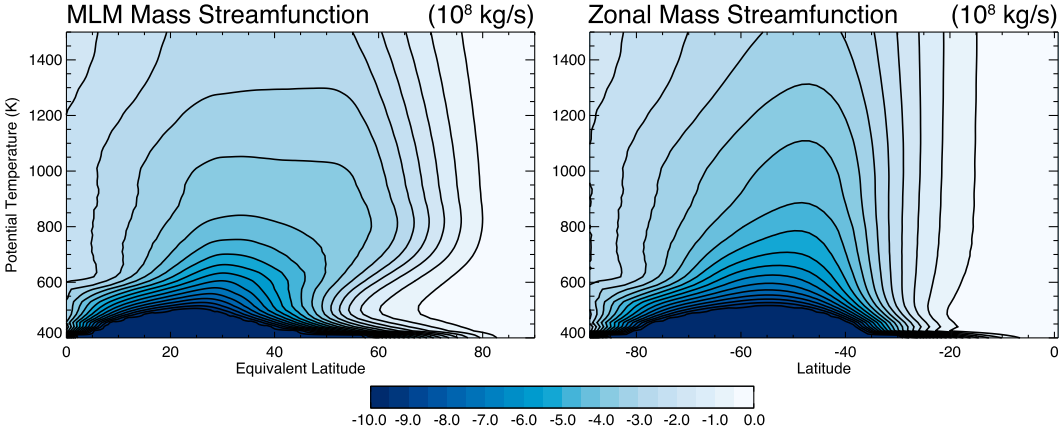


FIG. 7. Mass streamfunctions ($10^8\,kg\,s^{-1}$) calculated relative to (left) tracer contours (i.e., equivalent latitude) and (right) latitude circles.

significantly modified by large-scale stirring. The first key statement to be concluded from this analysis is that large-scale tracer transport, summarized in $K_{YY}$, is predominantly isentropic and a property of large-scale stirring; it is largely independent of the direction of dissipation (isentropic or diabatic). In practice, resolution limitations, and our choice of flow regime, rendered our simulations capable of confirming insensitivity to the nature of small-scale dissipation only in regions (the lower stratosphere) where eddy stirring is sufficiently strong.

The second key statement is that, despite considerations raised in the introduction in the context of Fig. 2, the tilting of stretching filaments by the baroclinic shear does not lead to augmented diabatic transport. The only impact of the eddy motions on diabatic diffusivity occurs through modulation of isentropic thickness. This could be important in situations where eddies strongly modulate static stability, and where modest augmentation of diabatic diffusion could be important. Note, however, that the discussions here are based on a constant small-scale diabatic diffusivity; if this is a turbulent process, small-scale mixing could be suppressed where static stability is locally increased, in which case $K_{ZZ}$ may be even less sensitive to eddy effects.

Our numerical simulations have focused on tracer transport in the atmosphere, but the theoretical developments are general and can be applied to all baroclinic geophysical flows large enough to be balanced. For example, oceanic tracers are also stretched into tilted filaments containing a mean aspect ratio of $f/N$. Smith and Ferrari (2009) simulated the cascade of thermohaline variance in a quasigeostrophic model and, similar to this work, showed that isotropic diffusive processes acting upon small vertical scales are sufficient to halt the laterally driven cascade of tracer variance, thus supporting the conclusions drawn here and highlighting the importance of compact vertical scales in the atmosphere and ocean.

Many dynamical models have been constructed with the assumption of horizontal dissipation of tracer variance. While our results indicate that these models have not correctly simulated the physical processes terminating the variance cascade, the equivalence of properly scaled isentropic or diabatic diffusion suggests that the error is not particularly egregious. Indeed, as long as a model includes appropriate horizontal processes, the termination of the cascade can be properly simulated with grossly inadequate vertical resolution. However, vertical processes cannot be neglected in models containing both isentropic and diabatic diffusion. Even though quasi-horizontal strain drives the cascade of tracer variance, adequate vertical resolution is necessary to appropriately represent the ultimate termination of the cascade.

*Acknowledgments.* The authors wish to thank Daniela Domeisen (University of Hamburg) and Gang Chen (Cornell University) for helpful discussions and assistance with model simulations. We also thank two anonymous referees. This work was supported by the National Science Foundation through Grant ATM-0852384.

## APPENDIX A

### The Advective Terms

Given $M(Q, \Theta, t) = S(\Theta)A_e(Q, \Theta, t)$ and $(\partial A_e/\partial Y)_\Theta = L(Y)$, we have $dM|_\Theta = SdA_e = SLdY$, and

$$\left.\frac{\partial}{\partial Q}\right|_\Theta = \left(\frac{\partial Q}{\partial Y}\right)_Z^{-1} \left.\frac{\partial}{\partial Y}\right|_z, \tag{A1}$$

$$\left.\frac{\partial}{\partial \Theta}\right|_Q = \frac{dZ}{d\Theta}\left(\left.\frac{\partial}{\partial Z}\right|_Y - \frac{\partial Q/\partial Z}{\partial Q/\partial Y}\left.\frac{\partial}{\partial Y}\right|_z\right). \tag{A2}$$

Now,

$$\begin{aligned}\left(\frac{\partial M}{\partial t}\right)_{Q,\Theta} &= -\left(\frac{\partial M}{\partial Q}\right)_\Theta \left(\frac{\partial Q}{\partial t}\right)_{Y,\Theta} \\ &= -SL\left(\frac{\partial Y}{\partial Q}\right)_\Theta \left(\frac{\partial Q}{\partial t}\right)_{Y,\Theta}.\end{aligned}$$

Hence (8) becomes

$$\begin{aligned}\left(\frac{\partial Q}{\partial t}\right)_Y &= \left(\frac{\partial M}{\partial Q}\right)_\Theta^{-1}\left(\frac{\partial}{\partial Q}\mathcal{M}\{\dot{q}\}\right)_\Theta \\ &\quad + \frac{1}{SL}\left(\frac{\partial Q}{\partial Y}\right)_\Theta \left(\frac{\partial}{\partial \Theta}\mathcal{M}\{\dot{\theta}\}\right)_Q \\ &= \langle \dot{q}\rangle + \frac{1}{SL}\left(\frac{\partial Q}{\partial Y}\right)_\Theta \left(\frac{\partial}{\partial \Theta}\mathcal{M}\{\dot{\theta}\}\right)_{\hat{Q}}\end{aligned} \tag{A3}$$

from (7). But, using (A2),

$$\begin{aligned}\frac{d\Theta}{dZ}\left(\frac{\partial}{\partial \Theta}\mathcal{M}\{\dot{\theta}\}\right)_Q &= \left(\frac{\partial}{\partial Z}\mathcal{M}\{\dot{\theta}\}\right)_Y \\ &\quad - \left(\frac{\partial Q/\partial Z}{\partial Q/\partial Y}\right)\left(\frac{\partial}{\partial Y}\mathcal{M}\{\dot{\theta}\}\right)_Z.\end{aligned}$$

Then (A3) becomes

$$\left(\frac{\partial Q}{\partial t}\right)_Y = \langle \dot{q}\rangle - V\left(\frac{\partial Q}{\partial Y}\right)_Z - W\left(\frac{\partial Q}{\partial Z}\right)_Y, \tag{A4}$$

where the nondivergent advecting velocity is

$$\mathbf{V} = (V, W) = \left( -\overline{\rho}^{-1} \frac{\partial}{\partial Z} \mathcal{M}\{\dot{\theta}\},\ \overline{\rho}^{-1} \frac{\partial}{\partial Y} \mathcal{M}\{\dot{\theta}\} \right),$$

where

$$\overline{\rho} = SL \frac{d\Theta}{dZ} = \frac{\partial M}{\partial Y} \frac{d\Theta}{dZ} \tag{A5}$$

is the mass density in $(Y, Z)$ space.

## APPENDIX B

### The Diabatic Diffusion Term

From (7),

$$\left( \frac{\partial M}{\partial Q} \right)_\Theta \langle \dot{q} \rangle = \frac{\partial}{\partial Q} \left( \mathcal{M}\{\dot{q}\} \right)_\Theta = \frac{\partial}{\partial Q} \left[ \iint \frac{\partial}{\partial \theta} \left( \kappa_d \sigma |\nabla\theta|^2 \frac{\partial q}{\partial \theta} \right) dA \right]_\Theta .$$

Now, using the identity

$$\frac{\partial}{\partial \Theta} \left( \iint X dA \right)_Q = \iint \frac{\partial X}{\partial \theta} dA - \frac{\partial}{\partial Q} \left( \iint X \frac{\partial q}{\partial \theta} dA \right)_\Theta = \iint \frac{\partial X}{\partial \theta} dA - \oint X \frac{\partial q}{\partial \theta} \frac{dl}{|\nabla_h q|}, \tag{B1}$$

we have

$$\begin{aligned} \left( \frac{\partial M}{\partial Q} \right)_\Theta \langle \dot{q} \rangle &= \frac{\partial}{\partial Q} \left[ \frac{\partial}{\partial \Theta} \left( \iint \kappa_d \sigma |\nabla\theta|^2 \frac{\partial q}{\partial \theta} dA \right)_\Theta + \oint \kappa_d \sigma |\nabla\theta|^2 \left( \frac{\partial q}{\partial \theta} \right)^2 \frac{dl}{|\nabla_\theta q|} \right]_\Theta \\ &= \frac{\partial}{\partial \Theta} \oint \kappa_d \sigma |\nabla\theta|^2 \frac{\partial q}{\partial \theta} \frac{dl}{|\nabla_\theta q|} + \frac{\partial}{\partial Q} \oint \kappa_d \sigma |\nabla\theta|^2 \left( \frac{\partial q}{\partial \theta} \right)^2 \frac{dl}{|\nabla_\theta q|} \\ &= \frac{\partial}{\partial \Theta} \left( \frac{\partial M}{\partial Q} \left\langle \kappa_d |\nabla\theta|^2 \frac{\partial q}{\partial \theta} \right\rangle \right) + \frac{\partial}{\partial Q} \left[ \frac{\partial M}{\partial Q} \left\langle \kappa_d |\nabla\theta|^2 \left( \frac{\partial q}{\partial \theta} \right)^2 \right\rangle \right]. \end{aligned}$$

Map this into $(Y, Z)$ space using (A1) and (A2), which, after some manipulation, gives

$$\langle \dot{q} \rangle = \frac{1}{\overline{\rho}} \frac{\partial}{\partial Y} \left[ \overline{\rho} \left( \frac{\partial Q}{\partial Y} \right)_\Theta^{-1} \left\langle \kappa_d |\nabla\theta|^2 \frac{\partial q}{\partial \theta} \left( \frac{\partial q}{\partial \theta} - \frac{\partial Q}{\partial \Theta} \right) \right\rangle \right]_Z + \frac{1}{\overline{\rho}} \frac{\partial}{\partial Z} \left( \overline{\rho} \frac{dZ}{d\Theta} \left\langle \kappa_d |\nabla\theta|^2 \frac{\partial q}{\partial \theta} \right\rangle \right)_Y . \tag{B2}$$

Now write $\partial q/\partial\theta = \partial Q/\partial\Theta + q'_\theta$. Then

$$\begin{aligned} \langle \dot{q} \rangle = {} & \overline{\rho}^{-1} \frac{\partial}{\partial Y} \left( \overline{\rho} \left[ \frac{\langle \kappa_d |\nabla\theta|^2 q'^2_\theta \rangle}{(\partial Q/\partial Y)^2} \frac{\partial Q}{\partial Y} + \frac{\langle \kappa_d |\nabla\theta|^2 q'_\theta \rangle}{(\partial Q/\partial Y)(d\Theta/dZ)} \frac{\partial Q}{\partial Z} \right] \right) \\ & + \overline{\rho}^{-1} \frac{\partial}{\partial Z} \left( \overline{\rho} \left[ \frac{\langle \kappa_d |\nabla\theta|^2 q'_\theta \rangle}{(\partial Q/\partial Y)(d\Theta/dZ)} \frac{\partial Q}{\partial Y} + \frac{\langle \kappa_d |\nabla\theta|^2 \rangle}{(d\Theta/dZ)^2} \frac{\partial Q}{\partial Z} \right] \right). \end{aligned} \tag{B3}$$

Together, and noting that $|\nabla\theta| \simeq \theta_z$, (A4) and (B3) lead directly to (11).

## APPENDIX C

### Proof That $\langle q'_\theta \rangle = 0$ When $\sigma = \sigma(\theta)$

If $\sigma$ is constant within the isentropic surface, we can write $\sigma = S(\Theta)$ and so, using (6),

$$SA_e = M = \iint \sigma \, dA = S \iint dA .$$

But, from (B1),

$$\frac{\partial}{\partial \Theta} \left( \iint dA \right)_Q = -\oint \frac{\partial q}{\partial \theta} \frac{dl}{|\nabla_h q|} = -\frac{1}{S} \oint \sigma \frac{\partial q}{\partial \theta} \frac{dl}{|\nabla_h q|} = -\frac{1}{S} \left\langle \frac{\partial q}{\partial \theta} \right\rangle \left( \frac{\partial M}{\partial Q} \right)_\Theta ,$$

and hence

$$\left\langle \frac{\partial q}{\partial \theta} \right\rangle = -\frac{(\partial A_e/\partial \Theta)_Q}{(\partial A_e/\partial Q)_\Theta} = \left(\frac{\partial Q}{\partial \Theta}\right)_{A_e}.$$

Hence,

$$\langle q'_\theta \rangle = \left\langle \frac{\partial q}{\partial \theta} \right\rangle - \left(\frac{\partial Q}{\partial \Theta}\right)_{A_e} = 0.$$

## REFERENCES


Abernathy, R., J. Marshall, M. Mazloff, and E. Shuckburgh, 2010: Enhancement of mesoscale eddy stirring at steering levels in the Southern Ocean. *J. Phys. Oceanogr.,* **40,** 170–184.

Allen, D. R., and N. Nakamura, 2001: A seasonal climatology of effective diffusivity in the stratopshere. *J. Geophys. Res.,* **106** (D8), 7917–7935.

Butchart, N., and E. E. Remsberg, 1986: The area of the stratospheric polar vortex as a diagnostic for tracer transport on an isentropic surface. *J. Atmos. Sci.,* **43,** 1319–1339.

Cerovecki, I., R. A. Plumb, and W. Heres, 2009: Eddy transport and mixing in a wind- and buoyancy-driven jet on the sphere. *J. Phys. Oceanogr.,* **39,** 1133–1149.

Gerber, E. P., 2012: Stratospheric versus tropospheric control of the strength and structure of the Brewer–Dobson circulation. *J. Atmos. Sci.,* **69,** 2857–2877.

——, and L. M. Polvani, 2009: Stratosphere–troposphere coupling in a relatively simple AGCM: The importance of stratospheric variability. *J. Climate,* **22,** 1920–1933.

Haynes, P., and J. Anglade, 1997: The vertical-scale cascade in atmospheric tracers due to large-scale differential advection. *J. Atmos. Sci.,* **54,** 1121–1136.

——, and E. Shuckburgh, 2000a: Effective diffusivity as a diagnostic of atmospheric transport: 1. Stratosphere. *J. Geophys. Res.,* **105** (D18), 22 777–22 794.

——, and ——, 2000b: Effective diffusivity as a diagnostic of atmospheric transport: 2. Troposphere and lower stratosphere. *J. Geophys. Res.,* **105** (D18), 22 794–22 810.

Held, I. M., and M. J. Suarez, 1994: A proposal for the intercomparison of the dynamical cores of atmospheric general circulation models. *Bull. Amer. Meteor. Soc.,* **75,** 1825–1830.

Kostrykin, S. V., and G. Schmitz, 2006: Effective diffusivity in the middle atmosphere based on general circulation model winds. *J. Geophys. Res.,* **111,** D02 304, doi:10.1029/2004JD005472.

Marshall, J., E. Shuckburgh, H. Jones, and C. Hill, 2006: Estimates and implications of surface eddy diffusivity in the Southern Ocean derived from tracer transport. *J. Phys. Oceanogr.,* **36,** 1806–1821.

Nakamura, N., 1996: Two-dimensional mixing, edge formation, and permeability diagnosed in an area coordinate. *J. Atmos. Sci.,* **53,** 1524–1537.

——, 1998: Leaky containment vessels of air: A Lagrangian-mean approach to the stratospheric tracer transport. *Dynamics of Atmospheric Flows: Atmospheric Transport and Diffusion Processes,* M. P. Singh and S. Raman, Eds., Advances in Fluid Mechanics, Vol. 18, WIT Press/Computational Mechanics, 193–246.

——, and J. Ma, 1997: Modified Lagrangian-mean diagnostics of the stratospheric polar vortices: 2. Nitrous oxide and seasonal barrier migration in the cryogenic limb array etalon spectrometer and SKYHI general circulation model. *J. Geophys. Res.,* **102** (D22), 25 721–25 735.

Orbe, C., and L. M. Polvani, 2012: Flux distributions as robust diagnostics of stratopshere-troposphere exchange. *J. Geophys. Res.,* **117,** D01302, doi:10.1029/2011JD016455.

Polvani, L. M., and P. J. Kushner, 2002: Tropospheric response to stratospheric perturbations in a relatively simple general circulation model. *Geophys. Res. Lett.,* **29,** doi:10.1029/2001GL014284.

Scinocca, J. F., and P. H. Haynes, 1998: Dynamical forcing of stratospheric planetary waves by tropospheric baroclinic eddies. *J. Atmos. Sci.,* **55,** 2361–2392.

Shuckburgh, E. F., and P. H. Haynes, 2003: Diagnosing transport and mixing using a tracer-based coordinate system. *Phys. Fluids,* **15,** 3342–3357.

Simmons, A. J., and D. M. Burridge, 1981: An energy and angular-momentum conserving vertical finite-difference scheme and hybrid vertical coordinates. *Mon. Wea. Rev.,* **109,** 758–766.

Smith, K. S., and R. Ferrari, 2009: The production and dissipation of compensated thermohaline variance by mesoscale stirring. *J. Phys. Oceanogr.,* **39,** 2477–2501.

Winters, K. B., and E. A. D'Asaro, 1996: Diascalar flux and the rate of fluid mixing. *J. Fluid Mech.,* **317,** 179–193.